UNDER REVIEW - ASL

On the need of bias adjustment for more plausible climate change projections of extreme heat

Maialen Iturbide[1] | Ana Casanueva[2] | Joaquín Bedia[2] | Sixto Herrera[2] | Josipa Milovac[3] | José Manuel Gutiérrez[3]

[1]Meteorology Group, Institute of Physics of Cantabria-University of Cantabria, Santander, 39005, Spain

[2]Meteorology Group, Dept. Applied Mathematics and Computer Sciences, University of Cantabria, Santander, 39005, Spain

[3]Meteorology Group, Institute of Physics of Cantabria, CSIC-University of Cantabria, 39005 Santander, Spain

Correspondence
Maialen Iturbide PhD, Meteorology Group, Institute of Physics of Cantabria-University of Cantabria, Santander, 39005, Spain
Email: miturbide@ifca.unican.es

Funding information

The assessment of climate change impacts in regions with complex orography and land-sea interfaces poses a challenge related to shortcomings of Global Climate Models (GCMs). Furthermore, climate indices based on absolute thresholds are specially sensitive to systematic model biases. Here we assess the effect of bias adjustment (BA) on the projected changes in temperature extremes by focusing on: (1) the number of annual days with maximum temperature above 35°C, and (2) above 40°C. To this aim, we present a global analysis of raw and BA CMIP5 projections under different Global Warming Levels (GWL). The resulting spatial pattern of the differences between raw and BA historical simulations is intensified with increasing future GWLs, mostly in the tropics. BA amplifies the magnitude of the climate change signal and strengthens multi-model agreement, unveiling a stronger effect of the correction in regions with an extensive land-sea interface or with complex orography, misrepresented by GCMs, achieving a more plausible representation of future heat extremes.

KEYWORDS
Climate impacts, climate indices, CMIP5, bias correction

Abbreviations: BA, bias adjustment; GWL, global warming level; GCM, global climate model

1 | INTRODUCTION

Each of the last three decades has been successively warmer at the Earth's surface than any preceding decade since 1850. In large parts of Europe, Asia and Australia the frequency of heat waves has likely increased due to climate change (IPCC, 2013). A significant proportion of total global land area has been identified as a persistent climate change hot-spot throughout the 21st century, like the Amazon, the Sahel and tropical West Africa, Indonesia, and the Tibetan Plateau (Diffenbaugh and Giorgi, 2012) and, in particular, South East Asia, North Africa, Australia or southern Europe (Suarez-Gutierrez, 2020). Accordingly, future heat extremes are very likely to be more frequent and longer-lasting (Collins et al., 2013; Horton et al., 2016), mainly as a direct consequence of the increase in mean temperature (Schär et al., 2004; Fischer and Schär, 2010).

The increased frequency and severity of extreme temperature events is associated to compound natural hazards such as droughts and wildfires, which cause damages to the natural systems and important economic losses in many sensitive areas of the world where climate projections point to increased impacts in the next decades (e.g. Bedia et al., 2015; Turco et al., 2018). Excessive heat has also a direct impact on biodiversity and crop yields, with large or small impacts depending on the development stage of the plant (Grotjahn, 2020). In particular, the negative impact of heat during the reproductive stage of the crops is a major threat to yield in many parts of the world (Deryng et al., 2014; Hatfield and Prueger, 2015).

Furthermore, heat exerts a direct impact on human well-being and human activities, emerging as an important threat in densely populated areas such as India, Southeast Asia and Africa (Zhao et al., 2015; Knutson and Ploshay, 2016; Rohini et al., 2016; Mora et al., 2017; Moda et al., 2019). Currently, the human thermoregulatory capacity of around a quarter of the world's population is affected by climate and such climatic conditions are projected to increase especially in the humid tropics (Mora et al., 2017). The consequences of major heat waves for human health have become apparent from the fatalities of recent events such as those in Chicago in 1995 (Changnon et al., 1996), Europe in 2003 –with more than 70,000 excess deaths across 12 European countries (Robine et al., 2008) and economic losses amounted to more than 13 billion euros (De Bono et al., 2004)– or Russia in 2010 (Barriopedro et al., 2011), among others.

The exposure-response relationship between temperature and heat-related impacts are usually built by either identifying "trigger points" or exposure limits linked, for instance, to the increased risk of health events (mortality, hospitalizations) associated directly and indirectly with heat (Petitti et al., 2016). Despite the common use of percentile-based indices, they have little bearing on impacts on human activities and agricultural products (Grotjahn, 2020). Consequently, many impact studies rely on absolute exposure limits, playing absolute temperature thresholds an important role in climate service provision. For instance, in heat-health warning systems, the issued heat warnings range from 30°C in Belarus to 38°C in Greece and up to 45°C in Phoenix (USA) (Casanueva et al., 2019). Also, staying below certain exposure limits –e.g. ambient temperature below 35°C (Kjellstrom et al., 2009b) and core body temperature below 38°C (Kjellstrom et al., 2009a)– reduces the risk of heat-related illness, but does not preclude the possibility of other adverse effects such as a loss of labour productivity (Casanueva et al., 2020b), for which lower thresholds can be established. In the same vein, thresholds are also used in agriculture for issuing warnings. For instance, maize pollen viability decreases with temperatures above 35°C and rice production ceases above 40°C (Hatfield and Prueger, 2015; Grotjahn, 2020, an references therein).

Given the common use of absolute thresholds to quantify heat extremes and their impacts, robust methodologies are needed in order to produce reliable climate change projections. However, the assessment of heat impacts in regions with complex orography, intricate coastlines and/or small islands poses a challenge related to the inherent shortcomings of Global Climate Models (GCMs), related to their coarse spatial resolution and limited ability to model

small-scale processes which depend on the orography and land-sea interactions (e.g. Sanjay et al., 2017; Karl et al., 1999; Peterson et al., 2001). As a result, the development of reliable climate change projections of heat extremes in such regions is essential to advance in mitigation and adaption strategies to face its impacts. Nevertheless, indices based on absolute thresholds need to be treated with caution, since they are largely sensitive to systematic model biases. The application of some sort of bias adjustment (BA) is thus required when absolute thresholds are examined (e.g. Zhao et al., 2015; Matthews et al., 2017; Li et al., 2020). BA thus serves to place all models on equal footing, at the expense of some additional uncertainty due to the method (Casanueva et al., 2020a). In particular, the extrapolation ability beyond the observed climate and the ability of the method for preserving the global warming trend are two key aspects influencing climate projections of temperature extremes. On the other hand, the raw projected change of indices based on absolute thresholds may be unrealistic or unreliable, and BA can provide an improvement and a more robust signal (Dosio, 2016), through the reduction of the multi-model ensemble spread (see e.g. Zhao et al., 2015).

The objective of this study is to assess the effect of BA on the projected changes in temperature extremes for different Global Warming Levels (GWLs). To this aim, we analyze GCM outputs from the Coupled Model Intercomparison Project Phase 5 (CMIP5) with the focus on two absolute threshold-based extreme temperature indices, namely the number of annual days with temperature above 35°C (TX35) and 40°C (TX40), using both historical and RCP8.5 experiment simulations. The main results are summarized at a regional level using the recently defined reference regions of the IPCC (IPCC-WGI regions, Iturbide et al., 2020).

2 | DATA AND METHODS

2.1 | Model data

Daily maximum temperature from 28 GCMs from CMIP5 (Taylor et al., 2012, curated version used for IPCC-AR5) was used in this work considering both the *historical* and *RCP8.5* experiments (see Table 1). All the simulations were downloaded from the IPCC Data Distribution Center (`https://www.ipcc-data.org/sim/gcm_monthly/AR5/index.html`; last accessed, 31 Dec 2019). For the sake of comparability, all simulations were interpolated to a common 2° grid. The common grids and land/sea masks used are available in the ATLAS GitHub repository[1].

The period 1986-2005 was considered as the historical baseline while +1.5°C, +2°C and +3°C GWLs (with respect to the pre-industrial 1850-1900 mean value, see e.g. Nikulin et al., 2018) were used for future projections. The corresponding time periods for each GCM are computed using 20-year moving windows. Table 1 shows the central years (n) of the 20-year window where the warming is first reached. The GWL period is thus taken as [n-9, n+10]. The use of a 20-year moving window is selected to be consistent with 20-year time slices typically used for future projections: the near-term (2021-2040), mid-term (2041-2060) and long-term (2081-2100). The reference GWLs (and additional supplementary materials and reproducibility scripts) are available in the ATLAS GitHub repository[2].

2.2 | Observational data

Daily maximum temperature of EWEMBI (EartH2Observe, WFDEI and ERA-Interim data Merged and Bias-corrected for ISIMIP, Lange, 2016) was used as the observational reference to calibrate the GCM output. This dataset was developed as part of the Phase 2b of the Inter-Sectoral Impact Model Intercomparison Project (ISIMIP2b; Frieler et al., 2017), being the observational reference for the calibration of the Global Climate Models considered in this initiative.

[1] `https://github.com/SantanderMetGroup/ATLAS`, doi:10.5281/zenodo.3688072

[2] `https://github.com/SantanderMetGroup/ATLAS/tree/master/warming-levels`

TABLE 1 CMIP5 global models (GCMs) used in the study (for historical and RCP8.5 scenarios) for run *r1i1p1* in all cases except (*) *r12i1p1*. Columns indicate the effective resolution (longitude/latitude), and the central years of the 20-year period defining warming levels at +1.5°C, +2°C, and +3°C (using RCP8.5 scenario). More details about CMIP5 models are availabe at `https://pcmdi.llnl.gov/mips/cmip5/`.

	Resolution (°)		Warming levels		
GCMs	**Lon**	**Lat**	**+1.5°C**	**+2°C**	**+3°C**
ACCESS1-0	1.88	1.25	2028	2041	2061
ACCESS1-3	1.88	1.25	2031	2042	2062
bcc-csm1-1	2.81	2.77	2007	2028	2059
bcc-csm1-1-m	1.13	1.11	2019	2036	2059
CanESM2	2.81	2.77	2012	2026	2049
CCSM4	1.25	0.94	2014	2030	2057
CESM1-BGC	1.25	0.94	2017	2033	2058
CMCC-CESM	3.75	3.68	2029	2041	2061
CMCC-CM	0.75	0.74	2029	2041	2060
CNRM-CM5	1.41	1.39	2030	2044	2067
CSIRO-Mk3-6-0	1.88	1.85	2034	2044	2064
EC-EARTH(*)	1.13	1.11	2018	2034	2060
GFDL-CM3	2.50	2.00	2022	2034	2054
GFDL-ESM2G	2.00	2.00	2037	2054	2080
GFDL-ESM2M	2.50	2.00	2036	2051	2081
HadGEM2-CC	1.88	1.25	2027	2039	2056
HadGEM2-ES	1.88	1.25	2023	2035	2054
inmcm4	2.00	1.50	2044	2057	2083
IPSL-CM5A-LR	3.75	1.89	2009	2025	2047
IPSL-CM5A-MR	2.50	1.27	2015	2030	2050
IPSL-CM5B-LR	3.75	1.89	2022	2037	2061
MIROC-ESM	2.81	2.80	2018	2030	2050
MIROC-ESM-CHEM	2.81	2.80	2020	2030	2052
MIROC5	1.41	1.40	2033	2048	2071
MPI-ESM-LR	1.88	1.86	2017	2036	2061
MPI-ESM-MR	1.88	1.86	2019	2038	2060
MRI-CGCM3	1.13	1.12	2041	2052	2076
NorESM1-M	2.50	1.89	2032	2048	2072

It is a global daily dataset with 0.5° horizontal resolution covering the period 1979-2016. It is based on different datasets depending on the variable considered. In particular, for maximum temperature E2OBS (Dutra, 2015) and ERA-Interim (Dee et al., 2011) were the references over land and ocean, respectively (see Table 1 in Frieler et al., 2017).

2.3 | Bias adjustment

Empirical quantile mapping (EQM) is a commonly-used BA method in climate change impact applications and consists in calibrating a transfer function over the control period to map the quantiles from the empirical cumulative distribution function of the model output onto the corresponding observed distribution. Here we use the implementation from Déqué (2007) which fits 99 empirical percentiles and uses constant extrapolation for out-of-sample values (i.e. values below and above the calibration range). Note that, by construction, EQM allows the correction of intensity-dependent biases, thus modifications to the raw signals are expected.

The EQM implementation applied here is similar to the method applied in the Cost Action VALUE intercomparison experiment (Gutiérrez et al., 2019), with a slight modification in the moving window size in order to alleviate the computational demand of the method for the global domain (the methods is applied on a monthly basis in this case). The method is implemented in the R package *downscaleR* (Bedia et al., 2020) through the function `biasCorrection`, using the optional arguments `method="eqm"` and `window=c(30,30)`. Further details and worked examples of the EQM application for absolute threshold, temperature-based climate indices are given in Iturbide et al. (2019) and companion materials.

In order to avoid spurious effects due to the scale gap between model and observations, EWEMBI was regridded to the same common 2° resolution grid used for the GCMs before calibrating the BA method. This way the downscaling effect is avoided, being thus BA used as a mere correction (see Casanueva et al., 2020a, for a discussion on this). The EQM was trained over the historical 1986-2005 period and subsequently apply to the 20-year GWL periods (Table 1) considering every land gridbox for each GCM separately. Finally, monthly values of TX35 and TX40 were calculated from both the raw and BA daily maximum temperature time series.

3 | RESULTS

3.1 | Model biases in the historical period

The TX35 ensemble maps exhibit significant differences over sizeable global land areas after BA application, highlighting the crucial importance of the BA step in the final outcomes (Figure 1). These differences (expressed as the absolute difference $BA - raw$, in days) are remarkable in the historical simulation, preeminently affecting the intertropical range, for which the bulk of land area is concentrated on Africa (with a positive difference up to 50 days) over the updated IPCC-WGI regions SAH, WAF, CAF, NEAF (see Fig. 4a), South America (mixed pattern with positive differences over NWS and SAM and mostly negative in NSA –Amazon Basin– and NES), Central America (SCA) and SE Asia (mostly negative in SAS) and Indonesia (positive in SEA and NAU regions). Some important differences are also found in some adjacent areas of the extratropic in North/South America (NCA/SES regions), Northern/Southern Africa (MED/SWAF), the Middle East (ARP, WCA) and Australia (CAU). The highlighted regions resemble the spatial pattern of CMIP5 biases in extreme values of mean temperature in previous studies (Zhao et al., 2015).

An orographic pattern of the difference between raw and BA maps is unveiled in some world areas (Figure 1). For instance, in South America positive differences are located over the major mountainous areas of the continent, namely

Andes and Brazilian highlands, while the negative differences are strengthened in low-lying areas of the Amazon (NSA) and Paraná (SES) River Basins. Conversely, a strong negative difference (nearly -40 days in the historical simulation) is found in the Tibetan Plateau, contrasting with the positive difference in southern India, both within the SAS region.

Tropical regions that are mostly insular (CAR in central America and SEA in SE Asia) also exhibit a strong sensitivity to BA application. For instance in the Caribbean, while the 35°C threshold is never reached, neither in the historical simulation, nor in the GWL projections, a significant increment is found in TX35 after BA application. This increment is also accentuated and locally very strong in many SEA islands (above +40 days/year).

3.2 | Future projections of extreme heat

The differences between raw and BA projections are increasingly reinforced for +1.5°C, +2°C and +3°C GWLs (Fig. 1), unveiling a progressive southward displacement over the extratropic towards South American, South African and Australian regions, with a consistent positive difference. A few exceptions to this general pattern occur, notably in SE America (SES) and north of the SAS region (SE Asia), adjacent to the Himalayan region, that reach a negative difference close to about -45/-35 days for the +3°C GWL respectively. In addition, the SEAF region (SE Africa and Madagascar) is the only one where BA has a very limited effect on the projected changes. Moreover, in the Amazon basin (NSA, SAM) the negative difference found in the historical simulation is inverted showing a strong positive increment for all GWLs.

As a result, the effect of the BA correction is strong on the resulting ensemble TX35 delta change maps, with reference to the historical period. These are presented in Figure 2 for the three different GWL future projections, unveiling a consistent pattern of signal amplification for the different GWLs. The multi-model agreement is also clearly improved after BA yielding more robust ensemble projections (reduced hatched areas). The effect of BA on the resulting delta change maps follows a similar pattern in the case of the TX40 index (Fig. 2 of supplementary material). Nevertheless, in this case the differences are mostly restricted to the tropical regions, where such high temperature threshold is projected to occur in the future, being the effect of the correction negligible elsewhere in terms of future delta changes (although still improving the ensemble spread).

In order to better understand the effect of BA, Figure 3 shows the SEA regional mean time series of the annual TX35. In this case, the climate change signal is largely reinforced after BA application. By the end of the 21st century, the projected delta change of the raw ensemble mean is of about +54 days/year (Fig. 3a), while it reaches about +216 days/year after BA (Fig. 3b), exhibiting a pronounced almost-linear trend until the last decades of the period, in which a stabilization becomes apparent. The ensemble spread is also more limited in the case of the BA projections, specially for TX40 (Fig. 3 of supplementary material), yielding a more robust ensemble projection than the raw version.

Finally, Figure 4 synthesizes the mean changes expected under +2°C GWL by aggregating the results region by region. This figure shows that the spatial patterns of differences for TX35 values when comparing the bias adjusted and raw data are similar for the historical and +2°C GWL periods (with positive and negative values), although intensified in the latter case. Moreover, the adjustment also affects the climate change signal with large positive differences (up to 50 days), which highlights the implications of bias adjustment in this type of threshold-based indices.

4 | DISCUSSION AND CONCLUSIONS

In general, fundamental model errors due to unrealistically represented processes cannot be improved by BA (Maraun et al., 2017), however the modification of the raw signal might be a desirable effect in some cases, such as intensity-

dependent biases (Gobiet et al., 2015; Ivanov et al., 2018) and applications using indices based on absolute thresholds (Dosio, 2016). The BA application of the TX35 and TX40 CMIP5 products here presented constitutes a suitable example of the latter.

For instance, several orographic features are visible when comparing the raw indices against the BA ensemble. The Himalaya and The Andes are relevant examples (Fig. 1). With this regard, it is noteworthy the added value of the correction since the observational datasets have a higher native resolution allowing for a better representation of orography, even after the degradation of its resolution prior to BA.

Similarly, over islands and predominantly insular regions like the Caribbean or Indonesia, the raw multimodel ensemble exhibits, in general, a weak linear trend throughout the 21st century. This trend is strongly reinforced after BA application (see e.g. Fig. 3, SEA region). This effect is therefore an actual "correction" of the raw model outputs, since the observational dataset (EWEMBI) is representing the land temperatures that the GCM simulates over the ocean, and therefore the BA method is capturing essential information for the insular territories that is not "seen" by the GCM, again attributable to the finer original resolution of the reference data used for correction.

These particular examples, focused on island territories and mountainous regions, demonstrate the need of bias adjustment for achieving a more plausible representation of future climate impacts, since observational references can aid to improve the poor GCM representation of these features due to their coarse original resolution. In the light of these results, the stronger and more rapid increase of the frequency of heat extremes in large parts of the world, including highly populated and vulnerable regions, highlights even further the need for adaptation and mitigation strategies.

This finding also paves the way for further analyses with alternative BA techniques for handling climate indices based on absolute thresholds. The positive temperature trends throughout the 21st century projections (particularly accentuated for the RCP8.5) pose a non-stationarity problem that is tackled in the case of the EQM approach using a constant correction for the outlying values of the latest percentile. However, alternative techniques may prove better suited to this particular extrapolation problem, and also in preserving the warming signal trends (Casanueva et al., 2020a)

acknowledgements

We acknowledge the World Climate Research Programme's Working Group on Coupled Modelling, which is responsible for CMIP, and we thank the climate modeling groups for producing and making available their model output. For CMIP the U.S. Department of Energy's Program for Climate Model Diagnosis and Intercomparison provides coordinating support and led development of software infrastructure in partnership with the Global Organization for Earth System Science Portals.

J.B., A.C. and S.H. acknowledge funding from the Project INDECIS, part of European Research Area for Climate Services Consortium (ERA4CS) with co-funding by the European Union Grant 690462.

J.M.G. and J.M. acknowledge the support of the Spanish Government through the project "Apoyo a unidades de excelencia María de Maeztu" (MdM-2017-0765).

references

Barriopedro, D., Fischer, E. M., Luterbacher, J., Trigo, R. M. and García-Herrera, R. (2011) The hot summer of 2010: Redrawing the temperature record map of europe. *Science*, **332**, 220–224.

Bedia, J., Herrera, S., Gutierrez, J., Benali, A., Brands, S., Mota, B. and Moreno, J. (2015) Global patterns in the sensitivity of burned area to fire-weather: implications for climate change. *Agricultural and Forest Meteorology*, **214–215**, 369–379.

Bedia, J., Baño Medina, J., Legasa, M. N., Iturbide, M., Manzanas, R., Herrera, S., Casanueva, A., San-Martín, D., Cofiño, A. S. and Gutiérrez, J. M. (2020) Statistical downscaling with the `downscaleR` package (v3.1.0): contribution to the value intercomparison experiment. *Geoscientific Model Development*, **13**, 1711–1735.

Casanueva, A., Burgstall, A., Kotlarski, S., Messeri, A., Morabito, M., Flouris, A. D., Nybo, L., Spirig, C. and Schwierz, C. (2019) Overview of existing heat-health warning systems in europe. *International Journal of Environmental Research and Public Health*, **16**.

Casanueva, A., Herrera, S., Iturbide, M., Lange, S., Jury, M., Dosio, A., Maraun, D. and Gutiérrez, J. M. (2020a) Testing bias adjustment methods for regional climate change applications under observational uncertainty and resolution mismatch. *Atmospheric Science Letters*, **n/a**, e978.

Casanueva, A., Kotlarski, S., Fischer, A. M., Flouris, A. D., Kjellstrom, T., Lemke, B., Nybo, L., Schwierz, C. and Liniger, M. A. (2020b) Escalating environmental summer heat exposure—a future threat for the european workforce. *Regional Environmental Change*, **20**.

Changnon, S. A., Kunkel, K. E. and Reinke, B. C. (1996) Impacts and responses to the 1995 heat wave: A call to action. *Bulletin of the American Meteorological Society*, **77**, 1497–1506.

Collins, M., Knutti, R., Arblaster, J., Dufresne, J., Fichefet, T., Friedlingstein, P., Gao, X., Gutowski, W., Johns, T., Krinner, G., Shongwe, M., Tebaldi, C., Weaver, A. and Wehner, M. (2013) Climate Change 2013: The Physical Science Basis. Contribution of Working Group I to the Fifth Assessment Report of the Intergovernmental Panel on Climate Change. In *[Stocker, T.F., D. Qin, G.-K. Plattner, M. Tignor, S.K. Allen, J. Boschung, A. Nauels, Y. Xia, V. Bex and P.M. Midgley (eds.)]*. Cambridge, United Kingdom and New York, NY, USA: Cambridge University Press.

De Bono, A., Giuliani, G. and Kluser, S.a nd Peduzzi, P. (2004) Impacts of summer 2003 heat wave in europe. *Tech. Rep. 1-4*, United Nations Environment Programme.

Dee, D. P., Uppala, S. M., Simmons, A. J., Berrisford, P., Poli, P., Kobayashi, S., Andrae, U., Balmaseda, M. A., Balsamo, G., Bauer, P., Bechtold, P., Beljaars, A. C. M., van de Berg, L., Bidlot, J., Bormann, N., Delsol, C., Dragani, R., Fuentes, M., Geer, A. J., Haimberger, L., Healy, S. B., Hersbach, H., Hólm, E. V., Isaksen, L., Kållberg, P., Köhler, M., Matricardi, M., McNally, A. P., Monge-Sanz, B. M., Morcrette, J.-J., Park, B.-K., Peubey, C., de Rosnay, P., Tavolato, C., Thépaut, J.-N. and Vitart, F. (2011) The era-interim reanalysis: configuration and performance of the data assimilation system. *Quarterly Journal of the Royal Meteorological Society*, **137**, 553–597.

Déqué, M. (2007) Frequency of precipitation and temperature extremes over France in an anthropogenic scenario: Model results and statistical correction according to observed values. *Global and Planetary Change*, **57**, 16–26.

Deryng, D., Conway, D., Ramankutty, N., Price, J. and Warren, R. (2014) Global crop yield response to extreme heat stress under multiple climate change futures. *Environmental Research Letters*, **9**, 034011.

Diffenbaugh, N. S. and Giorgi, F. (2012) Climate change hotspots in the CMIP5 global climate model ensemble. *Climatic Change*, **114**.

Dosio, A. (2016) Projections of climate change indices of temperature and precipitation from an ensemble of bias-adjusted high-resolution euro-cordex regional climate models. *Journal of Geophysical Research: Atmospheres*, **121**, 5488–5511.

Dutra, E. (2015) Report on the current state-of-the-art Water Resources Reanalysis. *Earth2observe deliverable no. d.5.1*, ECMWF - European Center for Medium-Range Weather Forecasts. URL: `"http://earth2observe.eu/files/Public%20Deliverables"`.

Fischer, E. M. and Schär, C. (2010) Consistent geographical patterns of changes in high-impact european heatwaves. *Nature Geoscience*, **3**.

Frieler, K., Lange, S., Piontek, F., Reyer, C. P. O., Schewe, J., Warszawski, L., Zhao, F., Chini, L., Denvil, S., Emanuel, K., Geiger, T., Halladay, K., Hurtt, G., Mengel, M., Murakami, D., Ostberg, S., Popp, A., Riva, R., Stevanovic, M., Suzuki, T., Volkholz, J., Burke, E., Ciais, P., Ebi, K., Eddy, T. D., Elliott, J., Galbraith, E., Gosling, S. N., Hattermann, F., Hickler, T., Hinkel, J., Hof, C., Huber, V., Jägermeyr, J., Krysanova, V., Marcé, R., Müller Schmied, H., Mouratiadou, I., Pierson, D., Tittensor, D. P., Vautard, R., van Vliet, M., Biber, M. F., Betts, R. A., Bodirsky, B. L., Deryng, D., Frolking, S., Jones, C. D., Lotze, H. K., Lotze-Campen, H., Sahajpal, R., Thonicke, K., Tian, H. and Yamagata, Y. (2017) Assessing the impacts of 1.5 degree c global warming – simulation protocol of the inter-sectoral impact model intercomparison project (isimip2b). *Geoscientific Model Development*, **10**, 4321–4345.

Gobiet, A., Suklitsch, M. and Heinrich, G. (2015) The effect of empirical-statistical correction of intensity-dependent model errors on the temperature climate change signal. *Hydrology and Earth System Sciences*, **19**, 4055–4066.

Grotjahn, R. (2020) Weather extremes that impact various agricultural commodities. In *[Castillo, F. and Wehner, M. and Stone, D. (eds.)] Extreme Events and Climate Change: A Multidisciplinary Approach*. John Wiley & Sons, Inc. for American Geophysical Union. In press.

Gutiérrez, J. M., Maraun, D., Widmann, M., Huth, R., Hertig, E., Benestad, R., Roessler, O., Wibig, J., Wilcke, R., Kotlarski, S., San Martín, D., Herrera, S., Bedia, J., Casanueva, A., Manzanas, R., Iturbide, M., Vrac, M., Dubrovsky, M., Ribalaygua, J., Pórtoles, J., Räty, O., Räisänen, J., Hingray, B., Raynaud, D., Casado, M. J., Ramos, P., Zerenner, T., Turco, M., Bosshard, T., Štěpánek, P., Bartholy, J., Pongracz, R., Keller, D. E., Fischer, A. M., Cardoso, R. M., Soares, P. M. M., Czernecki, B. and Pagé, C. (2019) An intercomparison of a large ensemble of statistical downscaling methods over europe: Results from the value perfect predictor cross-validation experiment. *International Journal of Climatology*, **39**, 3750–3785.

Hatfield, J. L. and Prueger, J. H. (2015) Temperature extremes: Effect on plant growth and development. *Weather and Climate Extremes*, **10**, 4 – 10. USDA Research and Programs on Extreme Events.

Horton, R., Mankin, J., Lesk, C., Coffel, E. and Raymond, C. (2016) A review of recent advances in research on extreme heat events. *Current Climate Change Reports*, **2**.

IPCC (2013) Summary for Policymakers, In: Climate Change 2013: The Physical Science Basis. Contribution of Working Group I to the Fifth Assessment Report of the Intergovernmental Panel on Climate Change. In *[Stocker, T.F., D. Qin, G.-K. Plattner, M. Tignor, S.K. Allen, J. Boschung, A. Nauels, Y. Xia, V. Bex and P.M. Midgley (eds.)]*. Cambridge, United Kingdom and New York, NY, USA: Cambridge University Press.

Iturbide, M., Bedia, J., Herrera, S., Baño-Medina, J., Fernández, J., Frías, M., Manzanas, R., San-Martín, D., Cimadevilla, E., Cofiño, A. and Gutiérrez, J. (2019) The r-based climate4r open framework for reproducible climate data access and post-processing. *Environmental Modelling & Software*, **111**, 42 – 54.

Iturbide, M., Gutiérrez, J. M., Alves, L. M., Bedia, J., Cimadevilla, E., Cofiño, A. S., Cerezo-Mota, R., Di Luca, A., Faria, S. H., Gorodetskaya, I., Hauser, M., Herrera, S., Hewitt, H. T., Hennessy, K. J., Jones, R. G., Krakovska, S., Manzanas, R., Marínez-Castro, D., Narisma, G. T., Nurhati, I. S., Pinto, I., Seneviratne, S. I., van den Hurk, B. and Vera, C. S. (2020) An update of ipcc climate reference regions for subcontinental analysis of climate model data: Definition and aggregated datasets. *Earth System Science Data Discussions*, **2020**, 1–16.

Ivanov, M. A., Luterbacher, J. and Kotlarski, S. (2018) Climate model biases and modification of the climate change signal by intensity-dependent bias correction. *Journal of Climate*, **31**, 6591–6610.

Karl, T., Nicholls, N. and Ghazi, A. (eds.) (1999) *CLIVAR/GCOS/WMO workshop on indices and indicators for climate extremes: Workshop summary.* Dordrecht: Springer: Weather and Climate Extremes.

Kjellstrom, T., Holmer, I. and Lemke, B. (2009a) Workplace heat stress, health and productivity – an increasing challenge for low and middle-income countries during climate change. *Global Health Action*, **2**, 2047. PMID: 20052422.

Kjellstrom, T., MSc, R. S. K., MSc, S. J. L., PhD, T. H. and PhD, R. S. J. T. (2009b) The direct impact of climate change on regional labor productivity. *Archives of Environmental & Occupational Health*, **64**, 217–227. PMID: 20007118.

Knutson, T. and Ploshay, J. (2016) Detection of anthropogenic influence on a summertime heat stress index. *Climatic Change*, **138**.

Lange, S. (2016) EartH2Observe, WFDEI and ERA-Interim data Merged and Bias-corrected for ISIMIP (EWEMBI). *Gfz data services*, Potsdam Institute for Climate Impact Research, Telegraphenberg A 31, 14473 Potsdam, Germany.

Li, D., Yuan, J. and Kopp, R. E. (2020) Escalating global exposure to compound heat-humidity extremes with warming. *Environmental Research Letters*, **15**, 064003.

Maraun, D., Shepherd, T. G., Widmann, M., Zappa, G., Walton, D., Gutiérrez, J., Hagemann, S., Richter, I., Soares, P. M. M., Hall, A. and Mearns, L. O. (2017) Towards process-informed bias correction of climate change simulations. *Nature Climate Change*, **7**, 764––773.

Matthews, T. K. R., Wilby, R. L. and Murphy, C. (2017) Communicating the deadly consequences of global warming for human heat stress. *Proceedings of the National Academy of Sciences*, **114**, 3861–3866.

Moda, Filho and Minhas (2019) Impacts of climate change on outdoor workers and their safety: Some research priorities. *International Journal of Environmental Research and Public Health*, **16**, 3458.

Mora, C., Dousset, B., Caldwell, I., Powell, F., Geronimo, R., Bielecki, C., Counsell, C., Dietrich, B., Johnston, E., Louis, L., Lucas, M., McKenzie, M., Shea, A., Tseng, H., Giambelluca, T., Leon, L., Hawkins, E. and Trauernicht, C. (2017) Global risk of deadly heat. *Nature Climate Change*, **7**.

Nikulin, G., Lennard, C., Dosio, A., Kjellström, E., Chen, Y., Hänsler, A., Kupiainen, M., Laprise, R., Mariotti, L., Maule, C. F., Meijgaard, E. v., Panitz, H.-J., Scinocca, J. F. and Somot, S. (2018) The effects of 1.5 and 2 degrees of global warming on Africa in the CORDEX ensemble. *Environmental Research Letters*, **13**, 065003. URL: `https://iopscience.iop.org/article/10.1088/1748-9326/aab1b1/meta`.

Peterson, T. C., Folland, C., Gruza, G., Hogg, W., Mokssit, A. and Plummer, N. (2001) Report on the Activities of the Working Group on Climate Change Detection and Related Rapporteurs 1998-2001. *Wmo, rep. wcdmp-47, wmo-td 1071*, WMO, Geneve, Switzerland.

Petitti, D. B., Hondula, D. M., Yang, S., Harlan, S. L. and Chowell, G. (2016) Multiple trigger points for quantifying heat-health impacts: New evidence from a hot climate. *Environmental Health Perspectives*, **124**, 176–183.

Robine, J.-M., Cheung, S. L. K., Roy], S. L., Oyen], H. V., Griffiths, C., Michel, J.-P. and Herrmann, F. R. (2008) Death toll exceeded 70,000 in europe during the summer of 2003. *Comptes Rendus Biologies*, **331**, 171 – 178. URL: `http://www.sciencedirect.com/science/article/pii/S1631069107003770`. Dossier : Nouveautés en cancérogenèse / New developments in carcinogenesis.

Rohini, P., Rajeevan, M. and Srivastava, A. K. (2016) On the variability and increasing trends of heat waves over india. *Scientific Reports*, **6**.

Sanjay, J., Krishnan, R., Shrestha, A. B., Rajbhandari, R. and Ren, G.-Y. (2017) Downscaled climate change projections for the hindu kush himalayan region using cordex south asia regional climate models. *Advances in Climate Change Research*, **8**, 185 – 198. URL: `http://www.sciencedirect.com/science/article/pii/S1674927817300436`. Including special issue on climate change in the Hindu Kush Himalaya.

Schär, C., Vidale, P., Lïthi, D., Frei, C., Häberli, C., Liniger, M. and Appenzeller, C. (2004) The role of increasing temperature variability in european summer heatwaves. *Nature*, **427**.

Suarez-Gutierrez, L. (2020) Hotspots of extreme heat under global warming. *Climate Dynamics*, **in press**.

Taylor, K. E., Stouffer, R. J. and Meehl, G. A. (2012) An overview of cmip5 and the experiment design. *Bulletin of the American Meteorological Society*, **93**, 485–498.

Turco, M., Rosa-Cánovas, J. J., Bedia, J., Jerez, S., Montávez, J. P., Llasat, M. C. and Provenzale, A. (2018) Exacerbated fires in Mediterranean Europe due to anthropogenic warming projected with non-stationary climate-fire models. *Nature Communications*, **9**. URL: http://www.nature.com/articles/s41467-018-06358-z.

Zhao, Y., Ducharne, A., Sultan, B., Braconnot, P. and Vautard, R. (2015) Estimating heat stress from climate-based indicators: present-day biases and future spreads in the CMIP5 global climate model ensemble. *Environmental Research Letters*, **10**, 084013.

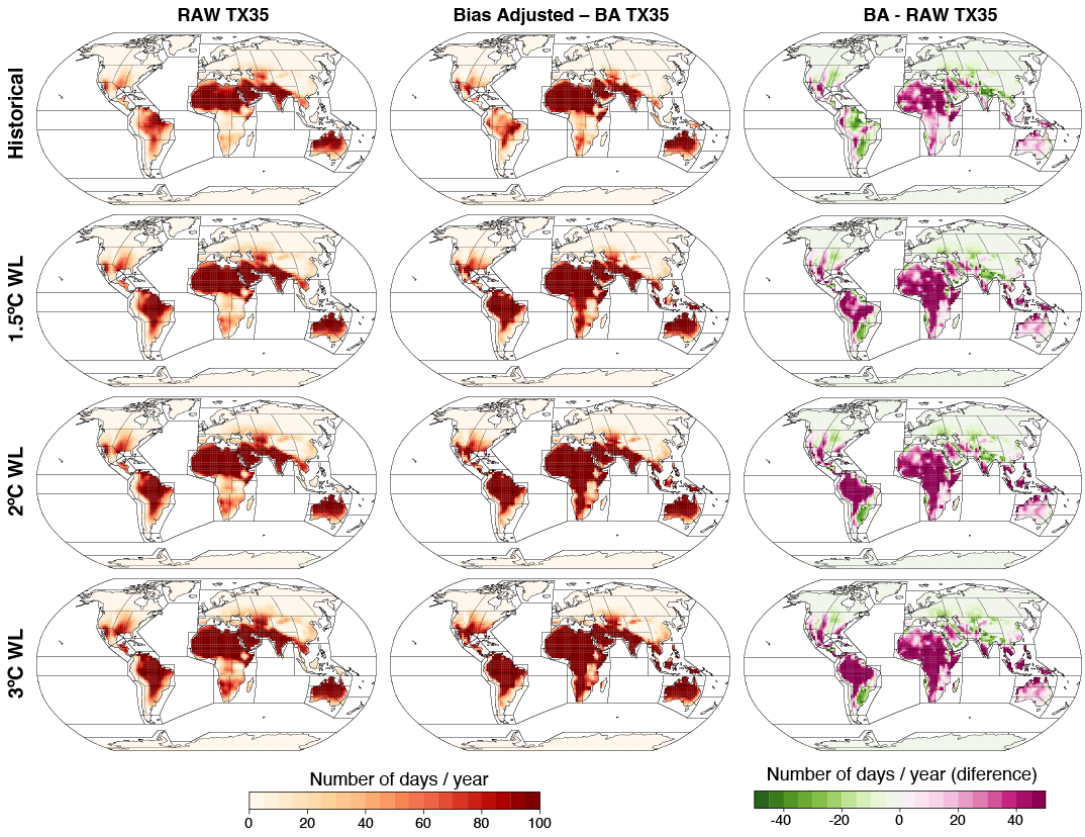

FIGURE 1 Number of mean annual days with maximum temperature above 35°*C* —TX35— for the raw (first column) and bias adjusted (second column). Results of the CMIP5 ensemble mean are shwon for the historical 1986-2005 period and the 1.5°*C*, 2°*C* and 3°*C* global warming levels (in rows). The last column shows the differences of bias adjusted and raw model outputs.

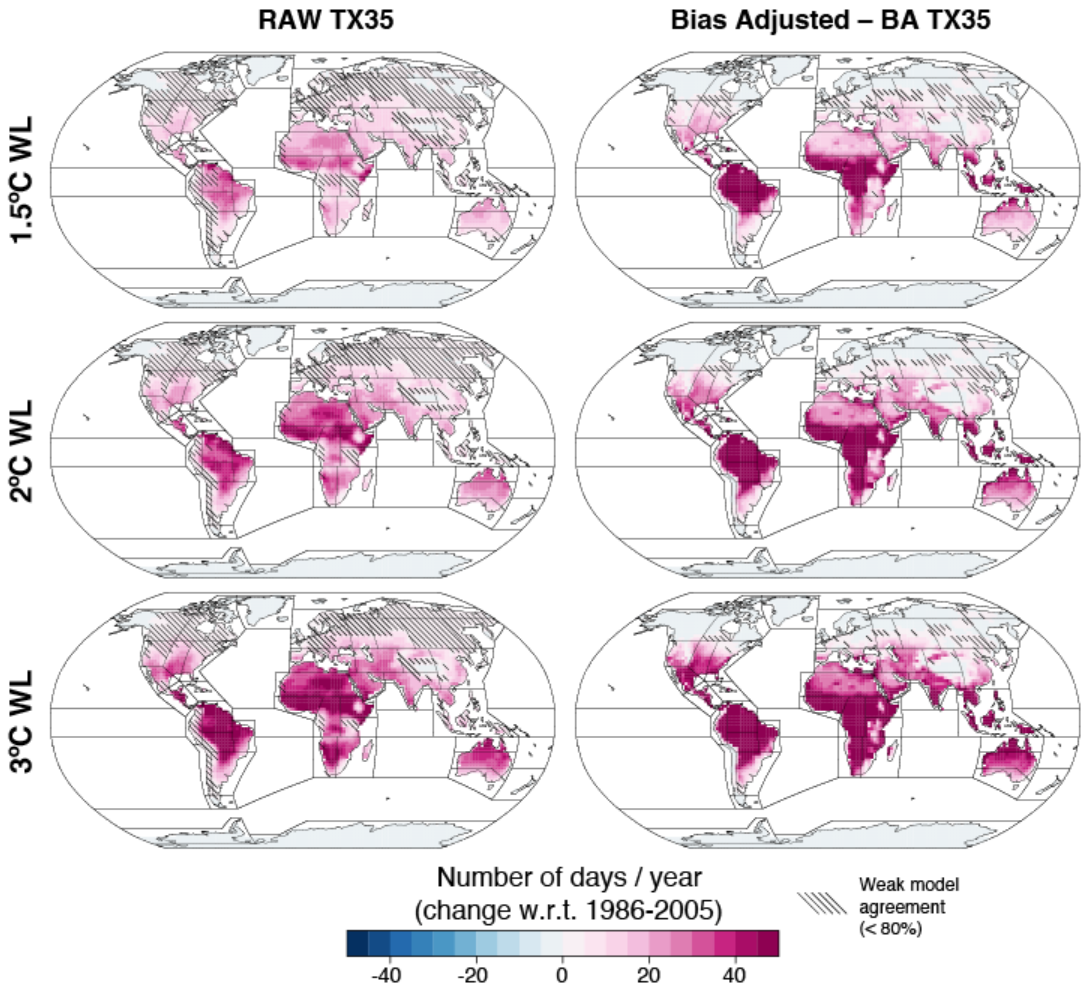

FIGURE 2 Changes in mean number of annual days with maximum temperature above 35°*C* —TX35— for three future 20-year periods corresponding to 1.5°*C*, 2°*C* and 3°*C* global warming levels (in rows) with respect to the historical 1986-2005 period. The first (second) columns shows the results corresponding to the raw (bias adjusted) model data. Hatching represents multi-model uncertainty (hatched areas correspond to weak model agreement, i.e. less than 80% of the models agreeing on the sign).

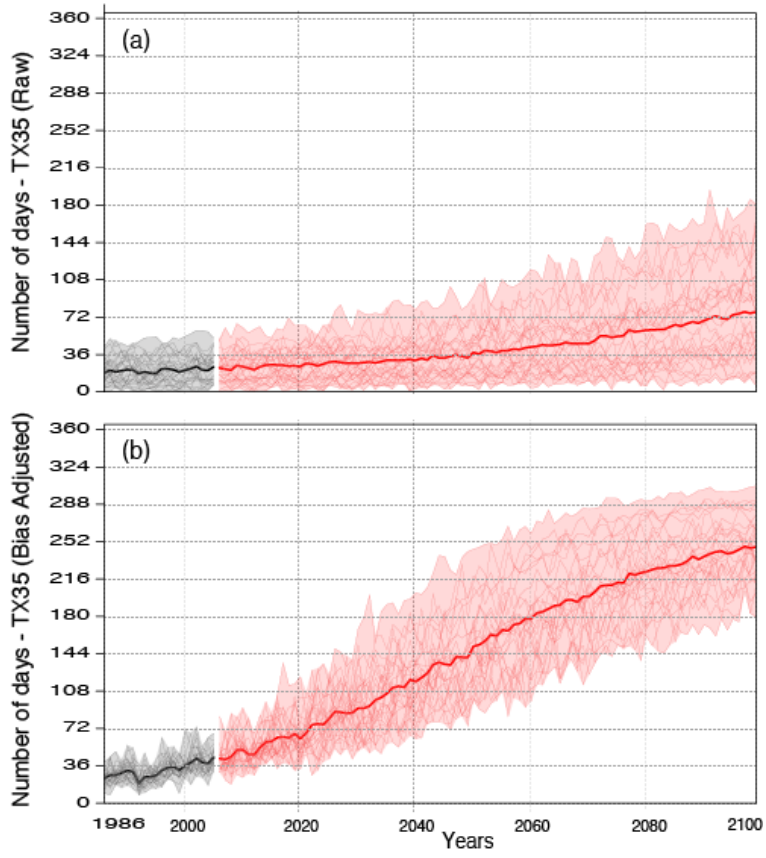

FIGURE 3 Historical and RCP8.5 time series of the individual models (thin lines) and the multimodel mean (solid lines) of regional TX35 for the SouthEast Asia (SEA) region for the (a) raw and (b) bias adjusted model data.

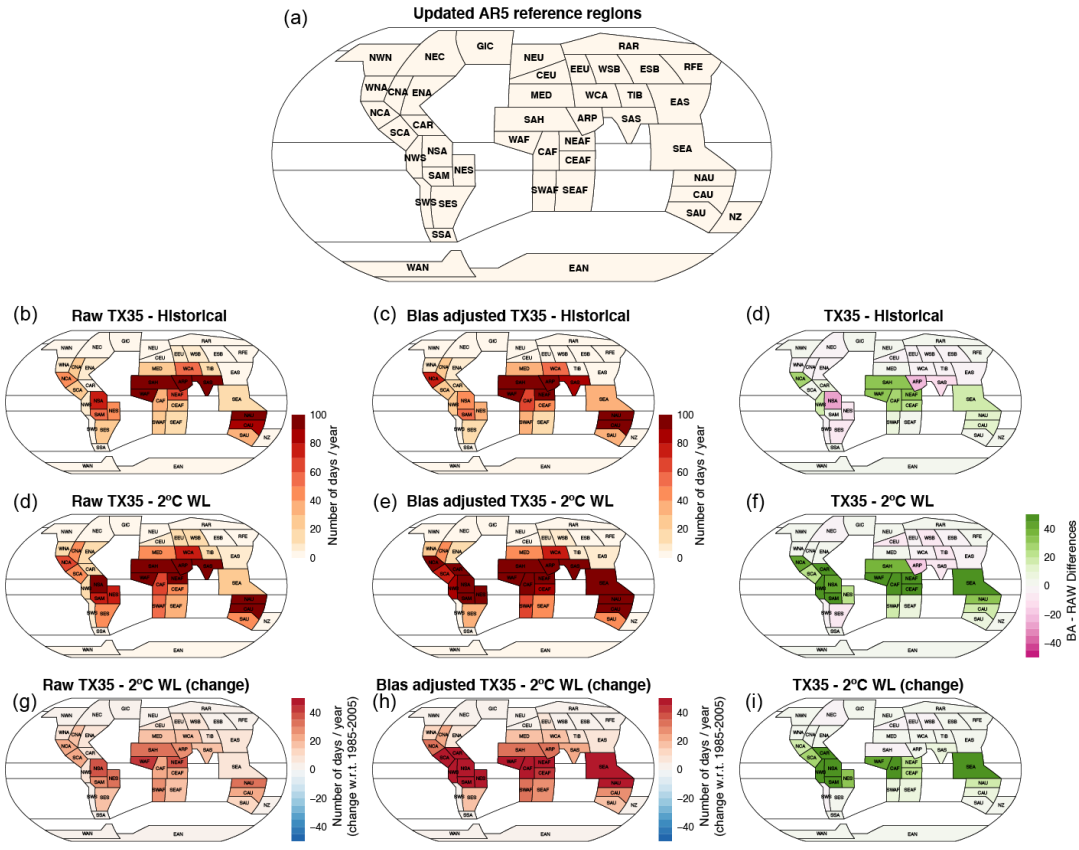

FIGURE 4 (a) Updated IPCC-WGI reference regions (see Iturbide et al., 2020, for details). Mean regional values of (gridbox) TX35 for the historical period from the raw data, the bias adjusted data and the differences between both for the historical (b-d), the $2^{\circ}C$ Warming Level (d)-(e), and for the changes, $2^{\circ}C$ w.r.t. the historical values (g-i).